Applied Catalysis B: Environmental 163 (2015) 223–232

Contents lists available at ScienceDirect

Applied Catalysis B: Environmental

journal homepage: www.elsevier.com/locate/apcatb

Selective catalytic reduction of NO_x by ammonia over phosphate-containing $Ce_{0.75}Zr_{0.25}O_2$ solids

Jun Yu [a], Zhichun Si [a,*], Lei Chen [a], Xiaodong Wu [a,b], Duan Weng [a,b]

[a] Graduate School at Shenzhen, Tsinghua University, Shenzhen 518055, China
[b] The Key Laboratory of Advanced Materials of Ministry of Education, School of Materials Science and Engineering, Tsinghua University, Beijing 100084, China

ARTICLE INFO

Article history:
Received 24 May 2014
Received in revised form 10 July 2014
Accepted 2 August 2014
Available online 12 August 2014

Keywords:
$Ce_{0.75}Zr_{0.25}O_2$
Zirconium phosphate
NH_3-SCR
Lattice oxygen

ABSTRACT

A zirconium phosphate @ $Ce_{0.75}Zr_{0.25}O_2$ (ZP/CZ) catalyst was synthesized by impregnating zirconium phosphates on $Ce_{0.75}Zr_{0.25}O_2$ microspheres. Catalysts with different structures were also synthesized by various methods to illustrate the structure advantage of ZP/CZ catalyst in selective catalytic reduction of NO_x by ammonia (NH_3-SCR). The catalysts were characterized by scanning electron microscope (SEM), X-ray diffraction (XRD), BET surface area, Infrared (IR) spectra, Ultraviolet-visible (UV–vis) spectroscopy, X-ray photoelectron spectroscopy (XPS), H_2-temperature programmed reduction (TPR) and diffuse reflectance infrared Fourier transformed spectra (DRIFTS) of NH_3/NO_x adsorption. ZP/CZ catalyst presents excellent catalytic activity at 250–450 °C with a good N_2 selectivity under high space velocity of 300,000 h^{-1}. Firstly, the zirconium phosphate provides adsorption sites for ammonia on the surface of the catalyst and the cerium sites in the core act as the redox sites for NO oxidation. The pre-combination of zirconium and phosphate can reduce the strong interactions between phosphates and cerium ions. Therefore, the mobility of surface lattice oxygen on $Ce_{0.75}Zr_{0.25}O_2$ catalyst is retained, which is essential to obtain a catalyst with high NH_3-SCR activity at low temperatures. Moreover, NH_4NO_3 has proved to be an important intermediate for the NH_3-SCR reaction on the surface of ceria based catalysts. The ZP/CZ catalyst preserves plenty of oxygen vacancies, facilitating the $Ce^{4+} \rightarrow Ce^{3+}$ redox circles and therefore promotes the nitrites/nitrates formation and desorption on catalyst. Two distinct adsorption sites for NH_3 and NO_x result in a close contact between ads-NH_3/NH_4^+ and ads-NO_3^-/NO_2^- species on ZP/CZ catalyst, which can react with NO rapidly with the participation of active surface lattice oxygen.

1. Introduction

Over the past decades, nitrogen oxides (NO, NO_2 and N_2O), which derive mainly from automobile exhausts and flue gases from the combustion of fossil fuels, lead to various environmental problems such as acid rain, photochemical smog, ozone depletion and greenhouse effects [1,2]. As the regulations against NO_x emissions have become stringent, many strategies have been exploited for NO_x removal. Among them, selective catalytic reduction of NO_x using ammonia as the reductant (NH_3-SCR) has been proven to be one of the most promising deNO_x technologies [3,4]. Nowadays, the most widely employed NH_3-SCR catalyst in the industry is V_2O_5-WO_3(or MoO_3)/TiO_2 which shows an excellent deNO_x performance and stability in the temperature range of 300–400 °C [5,6]. Transition-metal exchanged zeolites also exert satisfactory NH_3-SCR performances for deNO_x in a wide temperature range [6]. However, the toxicity of V_2O_5 and the high cost of zeolites restrain their commercial applications in deNO_x [7]. Recently, CeO_2-based NH_3-SCR catalysts, including CeO_2-TiO_2 [8–10] and CeO_2-ZrO_2 solid acid catalysts [11–13], have received much attention. However, the catalytic performances of ceria based catalysts still need to be improved to compete with the zeolite and vanadium catalysts.

Pure ceria proves active in NO oxidation and selective catalytic reduction of NO by NH_3, but shows rather poor SCR activity in the temperature range of 200–500 °C [14]. The high active surface oxygen of ceria catalyst results in NH_3 oxidation on the surface of the catalyst especially at high temperatures, leading to a decrease in NO_x conversion. It is generally accepted that the acid sites help to reduce the ammonia oxidation and promote the ammonia adsorption on the catalyst. Therefore, the N_2 selectivity of ceria catalysts can be enhanced by introducing the acid sites to ceria [9–13]. There are massive reports on CeO_2 catalysts modified by

* Corresponding author. Tel.: +86 755 26036861; fax: +86 755 26036417.
E-mail addresses: si.zhichun@sz.tsinghua.edu.cn, emsztsinghua@126.com (Z. Si).

http://dx.doi.org/10.1016/j.apcatb.2014.08.006
0926-3373/

Table 1
Textural features of the samples.

Sample	Ce (%)	Zr (%)	P (%)	Surface area (m^2/g)	Total pore volume (cm^3/g)	Average pore diameter (nm)
CP	50		50	42	0.449	38.1
CPZ	70	10	20	45	0.365	18.7
C/ZP	70	10	20	29	0.124	12.9
ZP/CZ	70	20	10	114	0.452	11.9
P/CZ	70	20	10	26	0.167	17.3

solid acids, such as MoO_3 [10,15], WO_3 [9,13], Nb_2O_5 [16], SO_4^{2-} [11,17] and PO_4^{3-} [12], because of both excellent redox ability and decent acidity coming from the interaction between cerium and acid components. In our previous report [12], $Ce_{0.75}Zr_{0.25}O_2$-PO_4^{3-} catalyst with a high hydrothermal stability shows over 80% NO_x conversion at 250–450 °C and can be regenerated completely by treated in air at 650 °C. Phosphates improve the ammonia adsorption and decrease the ammonia oxidation on the catalyst, leading to a high NH_3-SCR activity and a high N_2 selectivity of the $Ce_{0.75}Zr_{0.25}O_2$-PO_4^{3-} catalyst. Some phosphate-containing catalysts, such as $[Fe(H_2O)]_{0.20}(VO)_{0.80}PO_4$ [18], Cu- [19] and Co- [20] containing α-$Zr(HPO_4)_2$ (alumina pillared), also present remarkable SCR activities in a wide temperature region due to their high surface area and acidity arising from the layered or porous structure of phosphates. However, the structure–performance relationships of these catalysts, especially the phosphate-containing ceria catalyst, still need to be studied deeply.

As oxygen is one of the essential reactants in the standard SCR reactions, the ability of restoring and releasing oxygen is an important factor to determine the SCR activity of the catalyst. In this regard, ceria catalysts present an innate prospect because of the easier redox cycles from Ce^{4+} to Ce^{3+}. The surface oxygen was reported to be highly active in the NH_3/NO oxidation reaction due to its higher mobility than lattice oxygen, leading to the decrease of NH_3-SCR performance as the consequence of over-oxidation of NH_3 [11,21]. And the high mobility of lattice oxygen was reported to be essential for a catalyst with high NH_3-SCR activity [11,22,23]. Therefore, controlling the activity and mobility of surface/lattice oxygen via structure and component designing is very important for developing ceria-based NH_3-SCR catalysts.

The formation of $CePO_4$ (monazite), a Ce(III) phase, in vehicle aged three-way catalysts (TWC) has been pointed out as a cause of chemical deactivation [24–26]. The P_2O_5 that formed in the internal combustion engine enters the catalytic monolith by the exhaust gas and reacts with CeO_2 and $Ce_xZr_{1-x}O_2$ oxides to form cerium phosphate, in addition to other phosphate salts [24–26]. In the present study, zirconium phosphate rather than phosphate was used for ceria modification because the strong pre-combination between zirconium and phosphate could help to reduce the interaction between cerium and phosphate, and the layered structure of zirconium phosphate may also increase the surface area and acidity of the catalyst. Furthermore, catalysts with different structures were prepared and characterized to illustrate that the structure of zirconium phosphate @ $Ce_{0.75}Zr_{0.25}O_2$ catalyst is excellent for NH_3-SCR reaction.

2. Experimental

2.1. Materials and preparation method

All the materials (AR grade) for synthesizing the catalysts were from Aladdin Industrial Corporation, China.

$Ce_{0.75}Zr_{0.25}O_2$ powder was synthesized by the precipitation method. An appropriate amount of cerium (III) chloride heptahydrate and zirconyl chloride octahydrate were dissolved in deionized water to obtain the salt solution for precipitation. Afterwards, ammonia solution (25%) was added to the salt solution dropwise under magnetic stirring to obtain the precipitate until the pH of the mixed solution reaches 9 ~ 10. The mixture of liquid and precipitate was aged at 60 °C for 20 h, followed by spray drying at 200 °C to get the spherical powders. The powders were calcined at 500 °C for 3 h to get the $Ce_{0.75}Zr_{0.25}O_2$ microspheres. P/CZ and ZP/CZ catalyst were prepared by impregnating ammonia phosphate, or zirconyl chloride octahydrate and ammonia phosphate on $Ce_{0.75}Zr_{0.25}O_2$ powder according to the method in reference [12]. To illustrate the effects of mixing mode of CeO_2, ZrO_2 and phosphate on the performances, catalysts were prepared via different methods. CPZ catalyst was prepared by a sol–gel method [17]; C/ZP catalyst was prepared by impregnating ceria nitrate on pre-prepared zirconia phosphate; ZrP was prepared by the coprecipitation method according to the reference [27]. The components of catalysts are listed in Table 1.

2.2. Characterizations

Scanning electron microscope (SEM) images were obtained on a field emission SEM (FESEM, Hitachi S-4800) working at 10–20 kV.

Nitrogen adsorption isotherms were measured on Quantachrome NOVA apparatus. All the samples were degassed at 220 °C for 1 h prior to the nitrogen adsorption measurements. The BET surface area was determined by a multipoint BET method, using the adsorption data in the relative pressure ($P \cdot P_0^{-1}$) range of 0.05–0.3. The adsorption branch of nitrogen adsorption–desorption isotherms was used to determine the pore size distribution by the Barret–Joyner–Halender (BJH) method, assuming a cylindrical pore model.

The powder X-ray diffraction (XRD) experiments were performed on a Japan science D/MAX-2000 diffractometer employing Cu Kα radiation (λ = 0.15418 nm). The X-ray tube was operated at 40 kV and 40 mA. The X-ray powder diffractogram was recorded at 0.01° intervals in range of $20° < 2\theta < 80°$. The identification of the phases was made with the help of JCPDS cards (Joint Committee on Powder Diffraction Standards).

IR spectra of samples were collected on Nicolet iS10 apparatus equipped with a Smart ART appendix. The spectral resolution was $4\ cm^{-1}$.

The UV–vis diffuse reflectance spectroscopy (DRS) was obtained on a Scan UV–vis spectrophotometer (SCINNCO S-4100) equipped with an integrating sphere, using $BaSO_4$ as a reflectance sample.

The X-ray photoelectron spectroscopy (XPS) experiments were carried out on a PHI-QuanteaSXM system equipped with a monochromatic Al Kα X-rays under UHV (6.7×10^{-8} Pa). The binding energies were calibrated internally by the carbon deposit C 1s binding energy (BE) at 284.4 eV. Before tested, each sample was pre-treated at 105 °C in vacuum for 3 h.

H_2-TPR was performed on Micromeritics Auto Chem II. Prior to H_2-TPR experiment, 50 mg samples were treated by 10%O_2/He with a total flow rate of 50 ml min^{-1} at 500 °C for 30 min. The reactor temperature was raised to 1000 °C at a heating rate of 10 °C min^{-1} in H_2 (10 vol%)/Ar (50 ml min^{-1}).

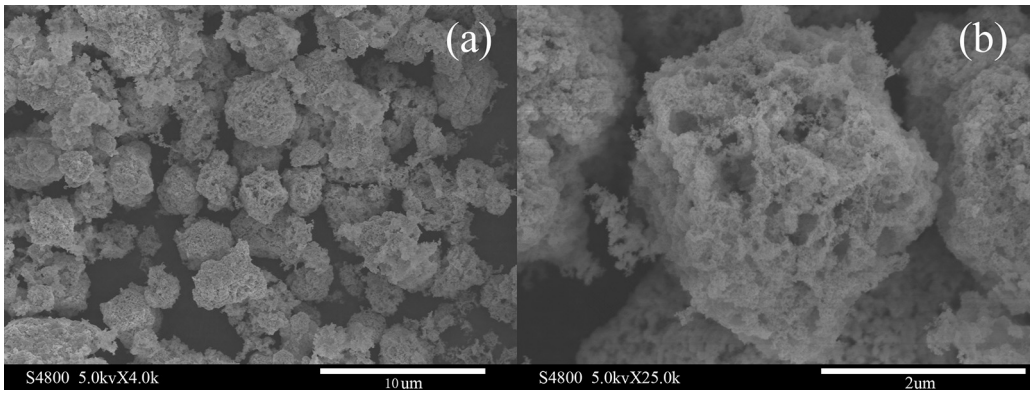

Fig. 1. The SEM images of $Ce_{0.75}Zr_{0.25}O_2$ powders.

DRIFTS of adsorbed species on NO_x pre-adsorbed catalyst arising from contact with NH_3 were recorded in the range of 4000–650 cm^{-1} using a thermo Nicolet 6700 FTIR spectrometer. The sample was heated up to 500 °C in a 20% (v/v) O_2/N_2 flow (100 ml min^{-1}) for oxidation treatment at 500 °C for 30 min. Then, the sample was cooled down to 250 °C, and subsequently purged by N_2 (100 ml min^{-1}) for 30 min for background collection. Afterwards, the gas mixture containing 1000 ppm NO + 5% O_2 in N_2 (100 ml min^{-1}) was flowed through the sample for 30 min to obtain the NO_x pre-adsorbed samples. After N_2 purging for 30 min, 1000 ppm NH_3 were introduced onto the pre-adsorbed samples for surface reaction. The spectra were collected in the whole procedure. A similar reaction process was adopted for the surface reaction between NO + O_2 and ads-NH_3. Also, NH_3 + NO + O_2 co-adsorption experiment was carried out, in which the gas mixture contains 1000 ppm NH_3 + 1000 ppm NO + 5% O_2 in N_2.

2.3. Activity measurement

The activity measurement for NO reduction with ammonia was carried out in a fixed bed reactor made of quartz tube. The reaction gas mixture consisted of 500 ppm NO, 500 ppm NH_3, 5% O_2, 5% H_2O and N_2 as balance. The total flow of the gas mixture was 0.5 l min^{-1} at a gas hourly space velocity (GHSV) of 3×10^5 h^{-1}. 0.2 g oxidized catalysts (0.1 ml) were measured from RT to 500 °C at a heating rate of 10 °C min^{-1}. The concentrations of nitrogen oxides and ammonia were measured at 120 °C by a thermo Nicolet iS10 FTIR spectrometer equipped with a quartz tube (6 mm i.d.). The oxidized catalyst samples were obtained by thermally treating the samples at 500 °C in a 10% (v/v) O_2/N_2 flow (500 ml min^{-1}) for 30 min. A similar reaction condition was used for the temperature-programmed oxidation of ammonia (NH_3-TPO) experiments, in which NO was not introduced into the gas mixture.

The O_2 shut-off test was carried out as follows: the oxygen supply was discontinued (1800–3000 s) when a steady SCR reaction (300–1800 s) was achieved at 250 °C. During this process, the NH_3 and NO_x concentrations were analyzed by Nicolet iS10. The total flow of the gas mixture was 0.5 l min^{-1} at a gas hourly space velocity (GHSV) of 3×10^5 h^{-1}.

In order to verify the possible accumulation of nitrates/nitrites on the catalyst during the NH_3-SCR reaction at 250 °C, the NH_3, NO, O_2 and H_2O supplies were replaced by N_2 to keep the total gas flow of 0.5 l min^{-1} when a steady SCR reaction was achieved in 7000 s, and then the reactor was heated up to 500 °C with the temperature ramping rate of 10 °C min^{-1}. The releases of NH_3 and NO_x were recorded to verify the deposited nitrates/nitrites on catalysts.

3. Results

3.1. Textural properties

Fig. 1 shows the typical SEM images of $Ce_{0.75}Zr_{0.25}O_2$ powders. The $Ce_{0.75}Zr_{0.25}O_2$ microspheres have a diameter of 1–5 μm and are formed by aggregation of primary nano-particles with a size of 10–20 nm. The morphologies of the catalysts are similar to $Ce_{0.75}Zr_{0.25}O_2$ powders no matter whether loading the phosphate or not (not shown). Many macro/meso-pores are found on the surface of particles in the amplified images (Fig. 1b).

The nitrogen adsorption/desorption isotherms of the catalysts are shown in Fig. 2 and Table 1. As shown in Table 1, the BET surface area of ZP/CZ catalyst is significantly higher than those of the other catalysts, indicating the formation of porous materials on $Ce_{0.75}Zr_{0.25}O_2$. The large N_2 uptake at low relative pressures reveals the presence of microporosity of ZP/CZ. The turning point of N_2-adsorbed volume on all catalysts are at 0.80 and the adsorbed volume of nitrogen further increases sharply under higher relative pressures, ascribed to the large mesorpores (>10 nm) in samples. Micropores and small mesopores predominate in ZP/CZ while large mesopores and macrospores predominate in CP. This leads to similar total pore volumes but large differences in BET surface area of CP and ZP/CZ. Also, some mesopores with a wide pore size distribution are observed in CPZ, which can be ascribed to the formation of layered phosphate-containing materials. Few mesopores are observed in P/CZ and C/ZP.

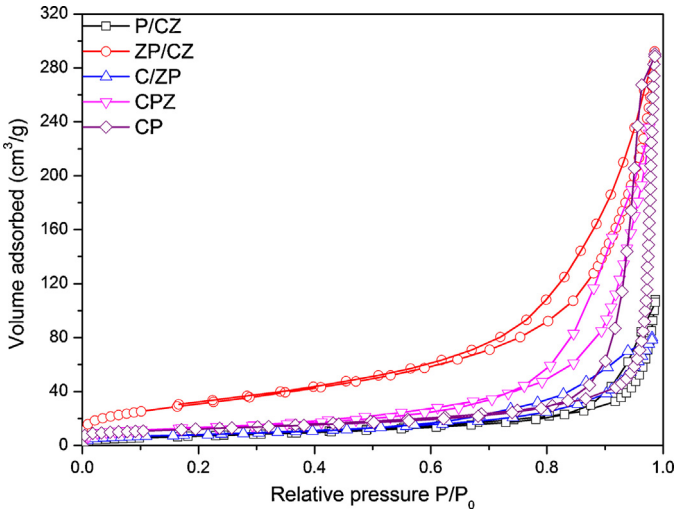

Fig. 2. N_2 adsorption–desorption isotherms.

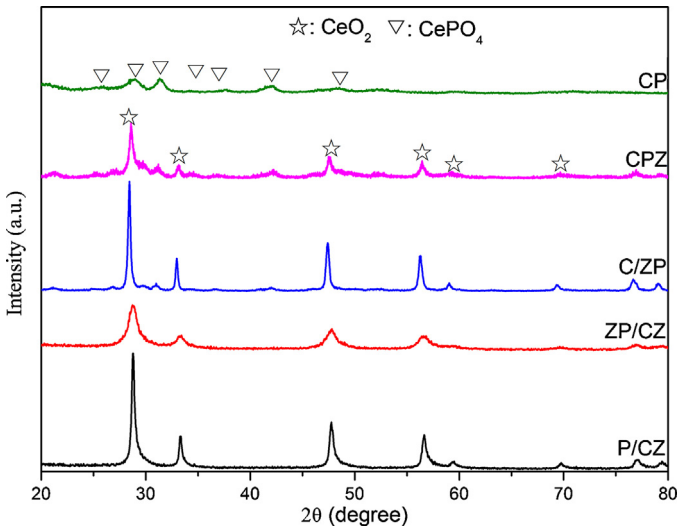

Fig. 3. XRD patterns of the catalysts.

XRD patterns of catalysts are shown in Fig. 3. The main characteristic peaks of the samples except CP are consistent with those of fluorite-like ceria. Only monoclinic cerium phosphate is detected in the XRD pattern of CP. Diffraction peaks of cerium phosphate are also observed in the XRD patterns of C/ZP and CPZ. No diffraction peaks associated with zirconia or zirconium phosphate are detected in all the samples, indicating that phosphate is prone to interact with cerium rather than zirconium. Therefore, the one pot synthesis of CeO_2-ZrO_2-PO_4^{3-} (CPZ) catalyst results in a strong interaction between cerium and phosphate, however, the interaction is restrained on the P/CZ and ZP/CZ catalysts. The lowest intensity of the ceria diffraction peaks on ZP/CZ suggests that ZP/CZ sample is in the lowest crystallization degree.

The IR spectra of the catalysts are shown in Fig. 4. Bands at 947–955, 991–993 and 1090–1092 cm^{-1} are ascribed to various phosphates on the catalysts [25]. The bands at 955, 993 and 1009–1092 cm^{-1}, in particular, align closely to those in monazite $CePO_4$ due to the asymmetric stretching of PO_3 terminal groups from orthophosphate [25,28,29]. The broad bands at 1043, 1028 and 1009–947 cm^{-1}, corresponding to P–O stretching vibration, indicate the poor crystallization of phosphates on ZP/CZ, P/CZ and ZP [30].

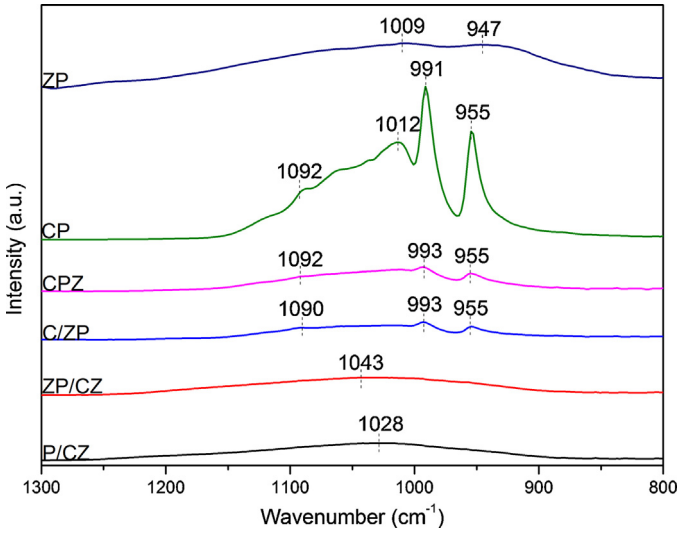

Fig. 4. IR of the samples.

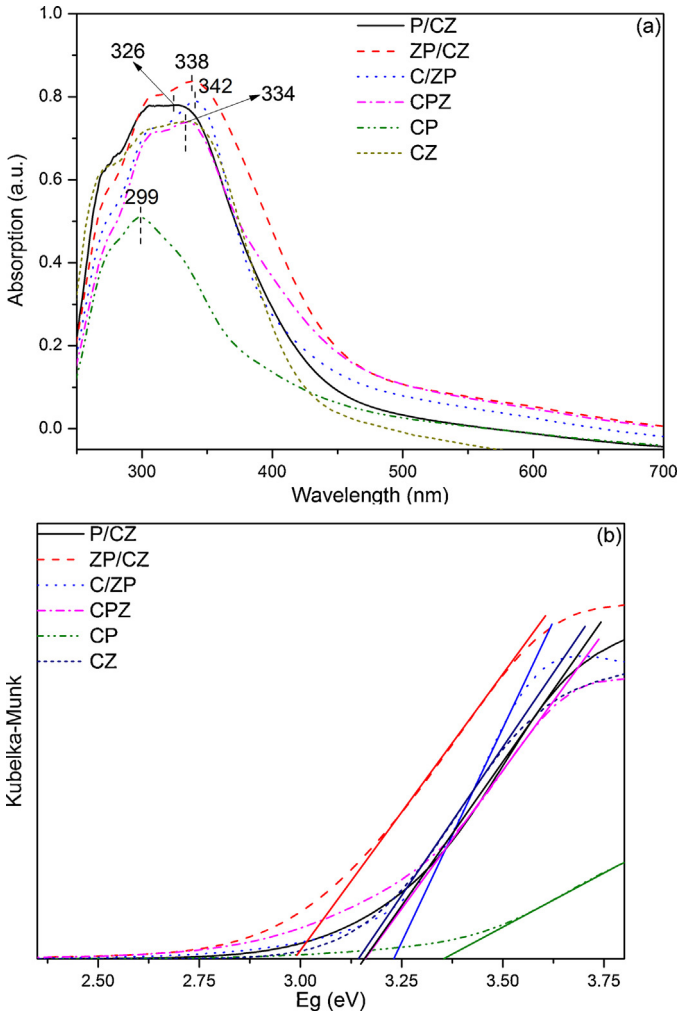

Fig. 5. UV–vis DRS (a) and band-gap energies (b) of the catalysts.

Fig. 5 shows the UV–vis spectra of the catalysts. All the catalysts exhibit strong absorption bands at about 300 and 340 nm due to the charge transfer transition from the O 2*p* to the Ce 4*f* orbital in CeO_2 [31,32]. Compared with the absorption band of $Ce_{0.75}Zr_{0.25}O_2$ (CZ) at 334 nm, this band shifts to higher wavelength when ceria is mixed with phosphate, indicating a perturbation of ceria edge by surface phosphates. It is noticed that PZ/CZ and CPZ present much stronger absorbance in the visible region (400–700 nm) than C/ZP, P/CZ, CP and CZ, which are associated with *d*–*d* transitions of reduced Ce^{n+} ($n<4$) centers, indicating that more quasi-free electrons on surface of these two catalysts than other catalysts. These results suggest the strong electron interaction between phosphate and CZ.

The relation between absorption coefficient (α) and band gap (E_g) can be written as $(\alpha h\nu)^n \propto h\nu - E_g$, where ν is the frequency, h is Planck's constant, and n is either 2 for a direct transition or 1/2 for an indirect transition [22]. The direct band gap energies of cerium catalysts were estimated by the plot of $(\alpha h\nu)^2$ versus photon energy ($h\nu$). As a result, the direct band-gap energies of CP, P/CZ, C/ZP, CPZ and PZ/CZ are 3.36, 3.16, 3.23, 3.16 and 2.99 eV, respectively, and ZP/CZ is smaller than the band gaps of bulk CeO_2 (3.15 eV) and CZ (3.13 eV). The red shifting of the absorption band edge is reported to be correlated with the formation of some localized band gap states owing to oxygen vacancy [33], which improves the redox property of the catalyst [22]. Therefore, it can be expected that the specific structure of PZ/CZ catalyst (amorphous zirconium

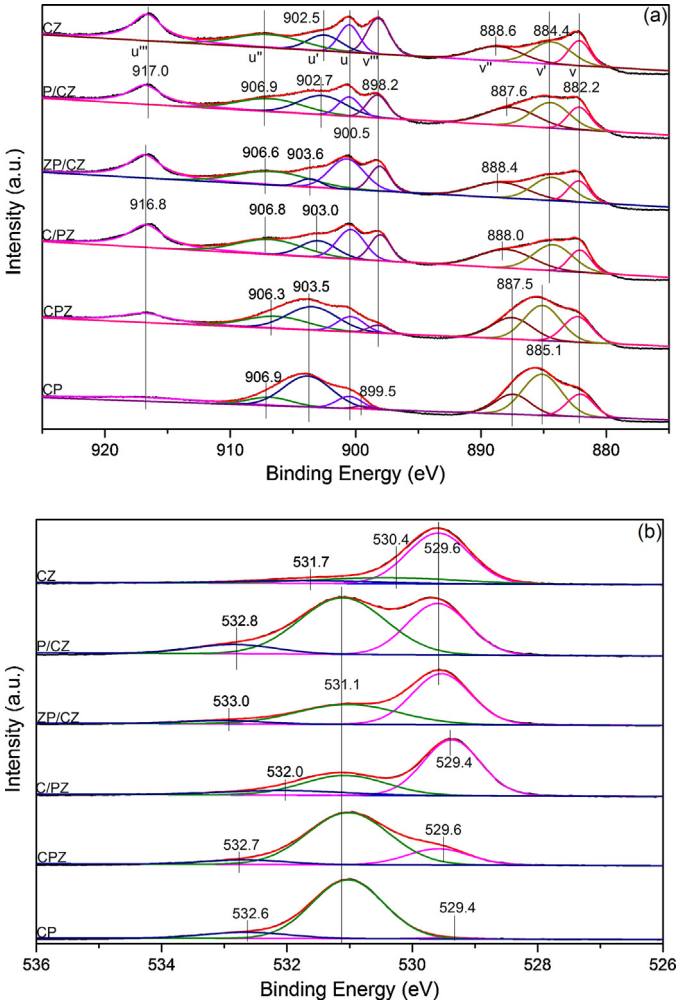

Fig. 6. XPS spectra of Ce 3*d* (a) and O 1*s* (b) of the catalysts.

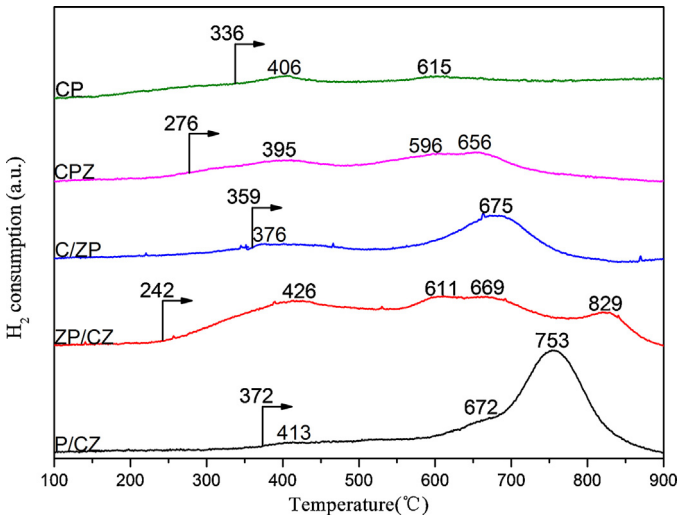

Fig. 7. H_2-TPR cures of the samples.

phosphate @ $Ce_{0.75}Zr_{0.25}O_2$) preserves plenty of oxygen vacancies on catalyst as well as introducing new acid sites on the catalyst (discussed later). The strong interaction between phosphate and ceria leads to the largest band gap of CP catalyst with few oxygen vacancies.

The XPS spectra of Ce 3d and O 1s of catalysts are shown in Fig. 6 and the element content of catalysts determined by XPS is shown in Table 2. As shown in Fig. 6(a), the Ce 3d band was resolved by eight peaks: the peaks labeled *u*, *u*″, *u*‴, *v*, *v*″ and *v*‴ represent the $3d^{10}4f^0$ state of Ce^{4+}, and the peaks labeled *u*′ and *v*′ represent the $3d^{10}4f^1$ state of Ce^{3+} [13]. The band energy of *u*′ on CZ is located at 902.5 eV, which shifts to higher band energy when cerium is mixed with phosphate (CP), which can be ascribed to the strong electron interaction between phosphate and cerium. The Ce^{3+} ions can be divided into two groups: (1) Ce^{3+} ions with loose contact with phosphates (oxygen vacancies), which can act as active sites for O_2 adsorption and activation; and (2) Ce^{3+} ions with strong interaction with phosphates (such as Ce^{3+} in $CePO_4$), which are difficult to participate in the redox reactions. It is seen in Table 2 that all the samples contain predominantly surface Ce^{4+}, with different amounts of Ce^{3+} depending on the preparation method. The increase in the concentration of surface Ce^{3+} component on the phosphate-containing catalysts except for ZP/CZ, compared with this on CZ, also proves the strong interaction between phosphate and cerium. However, the loading of zirconium phosphate reduces this effect significantly due to the pre-combination of phosphate with zirconium. The activities of SCR catalysts have been proved to be controlled by the redox properties of catalysts, especially at low temperature (<250 °C) [5]. Oxygen vacancies always directly participate in the redox circles of SCR reactions, and can provide more active sites [13,34,35]. Because cerium sites (Ce^{n+}) act as the only redox sites for the NH_3-SCR reaction on CeO_2-ZrO_2-PO_4^{3-} catalyst, catalyst owning easier transformation of $Ce^{3+} \leftrightarrow Ce^{4+}$ will have the high NH_3-SCR activity, especially at low temperatures. Therefore, it is difficult for the Ce^{3+} sites with strong interaction with phosphates to participate in the NH_3-SCR reaction at low temperatures.

Fig. 6(b) shows the O1s XPS spectra and the deconvolution results of all catalysts. The O1s XPS spectra can be deconvoluted into three distinct peaks: (1) one with lower binding energy assigned to lattice oxygen (O_L) in the metal oxides, (2) chemisorbed oxygen or/and weakly bonded oxygen species (O_C), and (3) peak at the highest binding energy is due to surface oxygen by hydroxyl species and/or adsorbed water species (O_S) on the surface [36,37]. As listed in Table 2 that ZP/CZ and C/ZP own significantly higher O_L/O_T ratio values than the other reference catalysts. The high concentration of lattice oxygen benefits the low-temperature NH_3-SCR activity of catalyst.

Table 2
The XPS results of the samples.

Sample	Ce content (%)	$Ce^{3+}/(Ce^{3+}+Ce^{4+})$ (%)	O/O_T (%)		
			O_L/O_T	O_C/O_T	O_S/O_T
CP	12.61	54.96	1.06	88.07	10.87
CPZ	12.68	40.47	18.12	75.51	6.37
C/ZP	16.49	24.13	59.57	30.37	10.7
ZP/CZ	12.05	17.66	57.22	37.78	5
P/CZ	8.71	30.95	35.72	55.51	8.77
CZ	13.83	22.70	72.45	19.19	8.37

3.2. H_2-TPR

The redox properties of the catalyst were characterized by H_2-TPR as shown in Fig. 7 and the related parameters are listed in Table 3. The H_2 consumption peaks over the catalysts are generally located at two temperature ranges: 250–500 and 500–900 °C, ascribed to the surface/sub-surface lattice oxygen and bulk lattice oxygen, respectively [38]. ZP/CZ catalyst presents the lowest starting temperature of H_2 consumption (242 °C) and the highest total H_2 consumption (61.42 μmol g^{-1}) at low temperatures (<500 °C).

Table 3
H_2-TPR parameters of the catalysts.

Catalysts	H_2 consumption (μmol g^{-1})		
	<500 °C	>500 °C	Total
CP	18	16	34
CPZ	52	26	78
C/ZP	1	160	161
ZP/CZ	61	76	137
P/CZ	3	291	294

It indicates that this catalyst has the highest amount of available surface/sub-surface lattice oxygen at low temperatures [38,39]. The surface reduction process involves reduction of Ce^{4+} to Ce^{3+} by the removal of lattice O^{2-} anions via oxygen vacancy generation. Meanwhile, surface oxygen vacancy generation triggers oxygen diffusion from the subsurface layers, and progressively proceeds deeper into the bulk until complete reduction of Ce(IV) to Ce(III) occurs [38]. The H_2 consumption by the catalysts at 250–500 °C follows the sequence of ZP/CZ > CPZ » CP > P/CZ; while that at 500–900 °C is in the order of P/CZ > ZP/CZ > CPZ » CP. These trends are very similar with the NO_x conversions at temperatures <300 °C and the NO_x conversions at temperatures >350 °C, which are shown in Fig. 8.

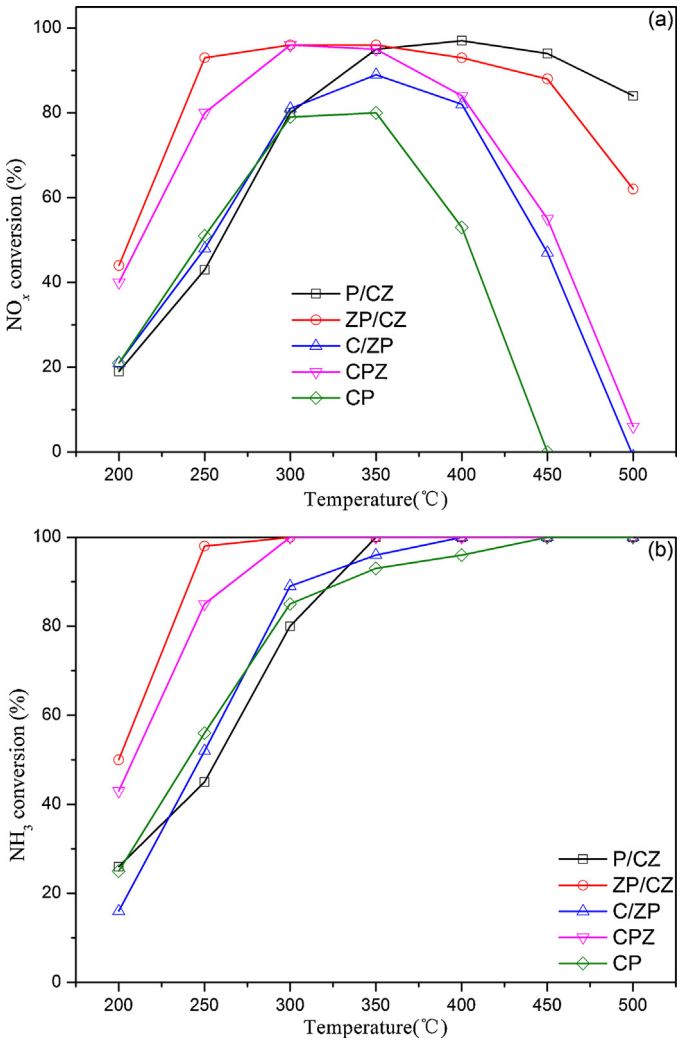

Fig. 8. NH_3-SCR activities of the catalysts: (a) NO_x conversions and (b) NH_3 conversions.

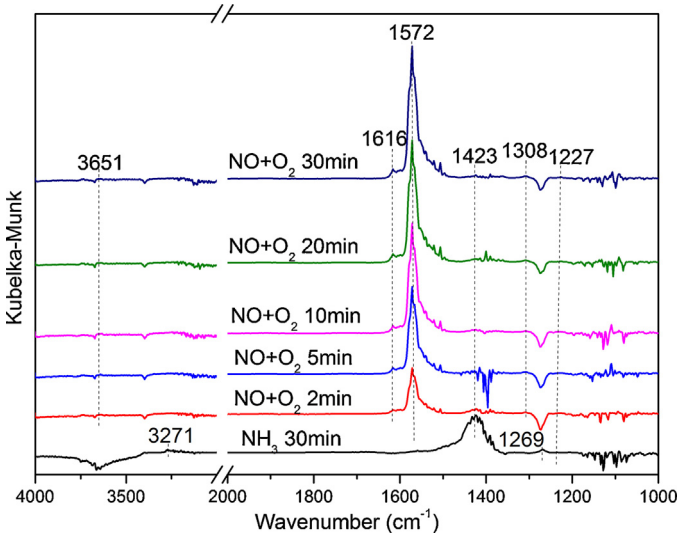

Fig. 9. DRIFT spectra of adsorbed species on the ZP/CZ catalyst arising from contact with 1000 ppm NO + 5% O_2 at 250 °C, N_2 balance. Pretreatment: 1000 ppm NH_3 pre-adsorbed followed by N_2 purging for 30 min.

3.3. Catalytic activities

3.3.1. SCR activities

The NH_3-SCR activities of catalysts are shown in Fig. 8. Generally, ZP/CZ shows a wider temperature window (NO_x conversions over 90%) of 250–450 °C than the other catalysts. At the temperatures below 300 °C, the NO_x conversions on catalysts follow the order of ZP/CZ > CPZ > CP > P/CZ, which is similar to the order of H_2 consumption at the temperatures lower than 500 °C, suggesting that the most available surface/sub-surface lattice oxygen may play an important role in the NH_3-SCR reaction. P/CZ catalyst owns the highest NO_x conversions in the high-temperature region (350–500 °C), suggesting that P/CZ is more suitable as a catalyst for high-temperature deNO_x. Both ZP/CZ and P/CZ catalysts show remarkably higher activities than other phosphate-containing catalysts. CPZ catalyst presents over 80% NO_x conversions in temperature region of 250–400 °C, which is similar with ZP/CZ, although the highest NO_x conversions of CPZ in the upper and lower temperature region of the temperature window are lower than ZP/CZ. It is interesting that $CePO_4$ also present good NH_3-SCR activity at 300–350 °C which was not reported before. The related mechanism of $CePO_4$ owning SCR activity is beyond the theme of this work.

Ammonia conversions reach nearly 100% at 450 °C over all the catalysts. If we compare Fig. 8(b) with Fig. 8(a), NH_3 conversion is found to follow the same trend of NO conversion initially until 400 °C. It implies that ammonia prefers reacting with NO_x-derived species (such as nitrate and nitrite) to with O_2 at low temperatures, and the latter becomes the dominant oxidizing agent for ammonia oxidation at high temperatures.

3.4. DRIFT studies

Because some important intermediates are very unstable or infrared inactive, we will not try to found all the possible intermediates but the reactivity of NO_x- and NH_3-derived species and the possible species accumulated on catalysts which will limit the kinetics of NH_3-SCR reaction.

3.4.1. Reaction between nitrogen oxides and ammonia ad-species

The DRIFT spectra of the NH_3 pre-adsorbed catalysts arising from contact with NO + O_2 at 250 °C are shown in Fig. 9. Several

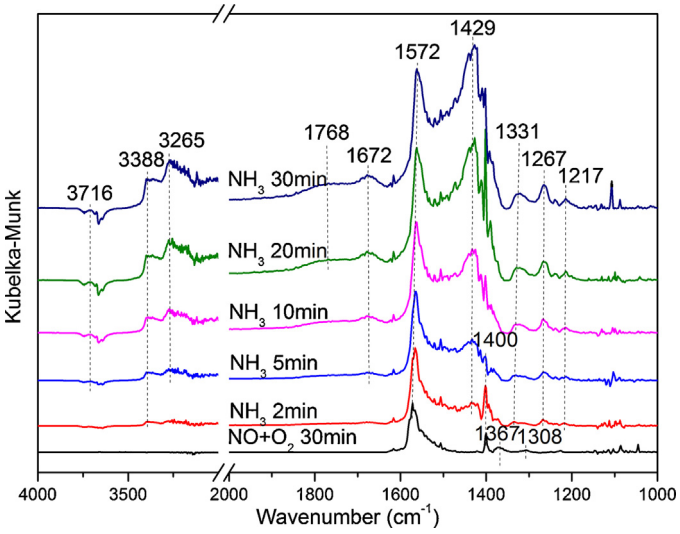

Fig. 10. DRIFT spectra of adsorbed species on the ZP/CZ catalyst arising from contact with 1000 ppm $NH_3 + O_2$ at 250 °C, N_2 balance. Pretreatment: 1000 ppm NO + 5% O_2 pre-adsorbed followed by N_2 purging for 30 min.

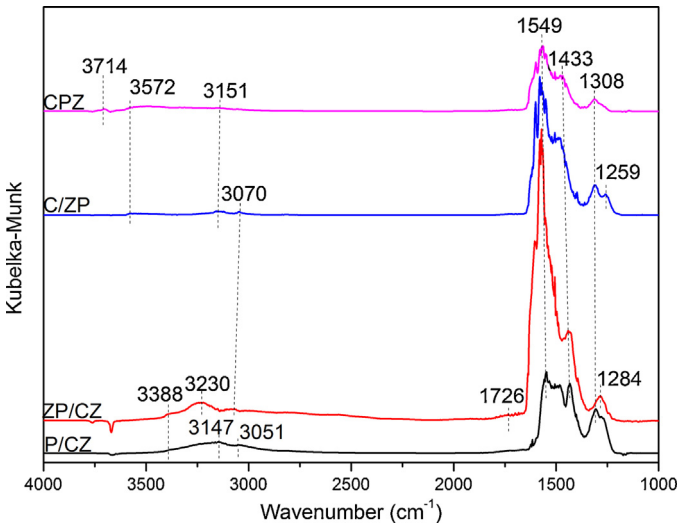

Fig. 11. DRIFT spectra of adsorbed species on the catalysts arising from contact with 1000 ppm NH_3 + 1000 ppm NO + 5% O_2 at 250 °C.

bands in the range of 1215–1227 (σ_s NH_3), 1423–1468 (σ_{as} NH_4^+) and 3000–3400 cm^{-1} (N–H stretching) are detected in the spectra obtained with ammonia adsorption at 250 °C followed by N_2 purging for 30 min, proving that there are plenty of Brønsted and Lewis acid sites on ZP/CZ [6–10]. Some negative bands at 3700 cm^{-1} are also observed, which could be assigned to the surface ammonia occupied O–H. The bands of ammonia derived species are very weak on C/ZP, indicating that the catalyst prepared by loading ceria on zirconium phosphate has a low acidity due to the surface coverage of basic rare earth oxide.

With the purging of NO + O_2, the bands of ammonia derived species decrease immediately via SCR reactions. Meanwhile, some bands of bridging nitrates (1227–1215 and 1606–1616 cm^{-1}), bidentate nitrates (1259–1271 and 1545–1572 cm^{-1}), monodentate nitrate (1271 and 1468–1479 cm^{-1}) and nitro compounds (1308–1321 cm^{-1}) are observed on the catalysts [6–10]. The relatively low intensities of bands ascribed to nitrates on ZP/CZ suggest that the structure of zirconium phosphate@ CeO_2-ZrO_2 helps to reduce the nitrate accumulation on the catalyst.

3.4.2. Reaction between ammonia and nitrogen oxides ad-species

The DRIFT spectra of the NO + O_2 pre-adsorbed catalysts from contact with NH_3 at 250 °C are shown in Fig. 10. Unlike the results in Fig. 9, no obvious changes in the bands of the pre-adsorbed NO_x species (1257–1265, 1309–1313, 1441–1483 and 1547–1572 cm^{-1}) can be observed after NH_3 treatment, indicating that the pre-deposited nitrates are relatively stable on all catalysts even after introducing NH_3. It is noticeable that the bands ascribing to Brønsted acid site bonded NH_4^+ ions (1429 cm^{-1}) and those on Lewis acid sites (3265–3388 and 1657–1265 cm^{-1}) appear immediately on the catalyst after introducing NH_3, indicating that there are distinct adsorption sites for the adsorption of ammonia and NO_x. However, the low-temperature NH_3-SCR activities of all catalysts present significant differences, which firmly indicates that ammonium nitrate participating in the NH_3-SCR reaction is the key prerequisite for NH_3-SCR activity of catalyst at low temperatures.

3.4.3. NO + NH_3 + O_2 co-adsorption

The DRIFT spectra of the adsorbed species from contact with NO + NH_3 + O_2 at 250 °C are shown in Fig. 11. Based on the results in Figs. 9–11, it can be concluded that there are mainly NH_3 (3572, 3147, 3070 and 1260 cm^{-1}), NH_4^+ (1726 and 1433 cm^{-1}) and nitrate (1549–1308 cm^{-1}) presented on surface of the catalyst although the bands of σ_s NH_3 and σ_{as} NH_4^+ strongly overlap the bands of nitrates. This result indicates that there are always ammonium nitrates deposited on the surface of the catalyst during the NH_3-SCR process. It is possible that different types of NH_4NO_3-like species are formed under different reaction conditions. It should be emphasized that the stretching band peak of NH_3 coordinated on Lewis sites on ZP/CZ are located at 3147 and 3070 cm^{-1}, consistent to the spectrum of pure NH_4NO_3 (3150 cm^{-1}) in Ref. [40], which are much lower than those in Fig. 10 (3388 and 3265 cm^{-1}) and those in Fig. 9 (3271 cm^{-1}), indicating the close contact of NH_3 with NO_3^- on ZP/CZ.

4. Discussion

4.1. Lattice oxygen mobility for NH_3-SCR reactions at low temperatures

Lietti [39] reported that the redox property of a catalyst was a key-factor in controlling the reactivity of V_2O_5-WO_3/TiO_2 de-NO_x catalysts at low temperatures. At low temperatures, the SCR reaction occurs via a redox mechanism that involves initially the participation of the lattice oxygen and then the re-oxidation of the reduced sites by gas-phase oxygen. In our previous report [11], the decreased surface active oxygen due to a surface covering effect on NiO-CeO_2-ZrO_2 catalyst by sulfate inhibited the ammonia oxidation. However, the improved mobility of catalyst lattice oxygen increased the reaction rate.

In this work, the NO_x conversions on catalysts follow the sequence of ZP/CZ > CPZ > CP ≈ P/CZ at the temperatures lower than 300 °C, which is similar to that of the H_2 consumption at the temperatures lower than 500 °C, indicating the readily available surface lattice oxygen plays an important role in the low temperature NH_3-SCR reaction. In order to consolidate this deduction, O_2 shut-off tests were performed to verify the roles of oxygen on NO and NH_3 conversions on various catalysts. When the NO and NH_3 concentrations reached a stable level, the inlet O_2 was shut off, and the consequent changes in the concentrations of NH_3 and NO_x were recorded. The results were shown in Fig. 12. It is remarkable that both NH_3 and NO concentration reached a stable level immediately (about 275 s) over P/CZ, CPZ and C/ZP when O_2 was shut off. However, on ZP/CZ, the NO and NH_3 concentrations cannot reach a stable level even when reacting for 1200 s. This result proves that

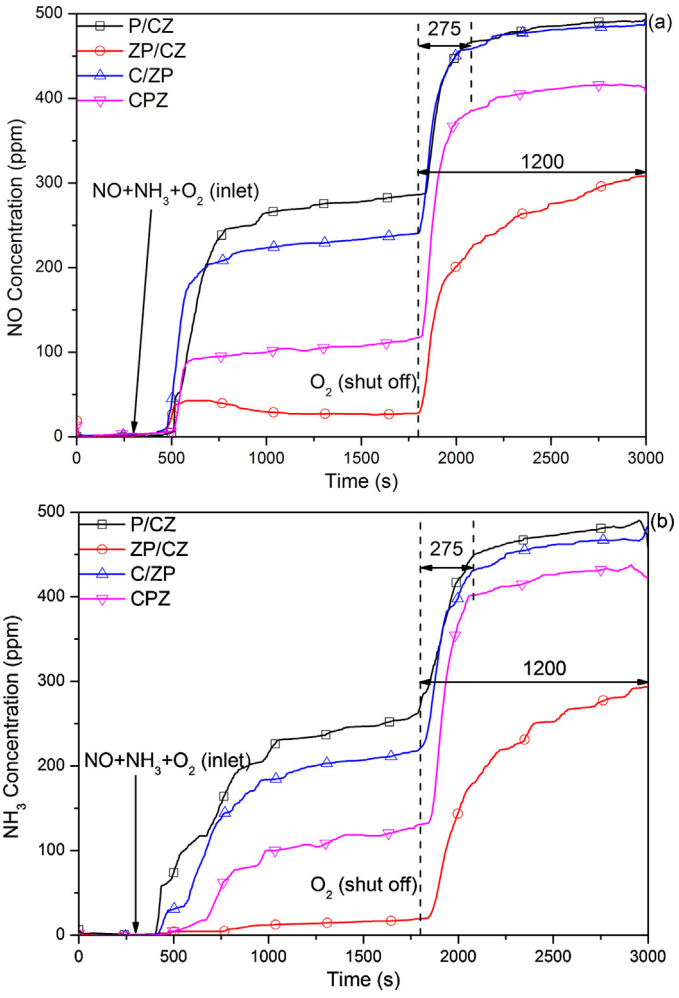

Fig. 12. NO (a) and NH_3 (b) concentration profiles in the O_2 shut-off test over various catalysts at 250 °C.

the lattice oxygen of catalyst participates in the low-temperature NH_3-SCR reaction.

The mobility of the surface lattice oxygen of ceria is mainly determined by the surface defects of the catalyst which can provide major transfer channels for surface oxygen (O^{2-}, O^-) and lattice oxygen (O^{2-}) [23]. Because cerium sites act as the only redox sites for NH_3-SCR on CeO_2-ZrO_2-PO_4^{3-} catalyst, catalyst owning easier transformation of $Ce^{3+} \leftrightarrow Ce^{4+}$ will have high NH_3-SCR activity especially at low temperatures. According to the XPS and H_2-TPR results, the strong bond between cerium and phosphate stabilizes the Ce^{3+} and inhibits the transfer of $Ce^{3+} \leftrightarrow Ce^{4+}$, which is considered as the main route of phosphate poisoning of three-way catalysts [24]. When Ce(III) phosphate is deposited on the surface of Ce–Zr oxide particles, the cycling of Ce^{4+}/Ce^{3+} redox pairs is still possible in the underneath CeO_2–ZrO_2 mixed oxide but the cerium phosphate layer blocks and inhibits the reduction and re-oxidation. This effect will not be a key factor for the catalyst working at the high temperatures, which explains its high NH_3-SCR activity at 350–500 °C. Loading zirconium phosphate on $Ce_{0.75}Zr_{0.25}O_2$ can reduce the strong interaction between phosphate and cerium in addition to introducing acid sites on surface of $Ce_{0.75}Zr_{0.25}O_2$. Therefore, ZP/CZ catalyst exhibits significantly higher NH_3-SCR activity than the other catalysts at low temperatures (<350 °C). However, the active surface lattice oxygen will also lead to the over oxidation of ammonia at high temperatures, leading to the decrease in NO_x conversion, which is the main reason for PC/CZ having lower NO_x conversions than P/CZ at 400–500 °C.

C/PZ catalyst, with zirconium phosphate as the support and ceria on the surface, exhibits much lower NO_x conversions in the whole temperature region, although its surface lattice mobility is comparable with the PZ/CZ catalyst. This result means that acidic surface is also essential to a catalyst with high NH_3-SCR activity besides the mobility of active lattice oxygen.

4.2. Effect of NH_3/NO_x adsorption, and NH_3-SCR reactions

Based on the DRIFTS results, nitrates and nitrites are prone to deposit on ceria catalyst, consistent to our previous reports [10–12]. If these deposited nitrates/nitrites cannot participate in the NH_3-SCR reaction at low temperatures, they may poison the catalyst. The result was further verified by the transient methods. The obtained NO_x and NH_3 concentration profiles in the NO and NH_3 shut off test were shown in Fig. 13. It is noticeable that P/CZ, C/PZ and CPZ present a slight increase in the NO concentration with prolonging the reaction time, suggesting the poisoning effect of the nitrate/nitrite accumulation on catalyst. A small amount of NO_2 evolved from the decomposition of ads-nitrates is detected with increasing the temperature, consisting with the DRIFT results. However, ZP/CZ catalyst shows a marvelous resistance to this poison effect.

Another interesting phenomenon is that there was remarkable ammonia storage on all phosphate-containing catalysts besides ZP/CZ along with the release of NO_2 at the very beginning of elevating the temperature, due to the decomposition of NH_4NO_3 like species (denote them as NH_4NO_3 for simplicity) deposited on those catalysts (Equation (1)). This result strongly suggests that NH_4NO_3 is an important intermediate in the NH_3-SCR reaction on ZP/CZ catalyst. The decomposition of NH_4NO_3 has been studied [40,41]. It was reported that the presence of ads-NH_3 and ads-NO_3^-/NO_2^- species results in the formation of ammonium nitrate (Equation (2)) which was a terminal product only in the absence of a suitable reducing agent [40,41]. When NO is included in the feed, ammonium nitrate can be reduced to ammonium nitrite and then decomposed to N_2 (Equation (3)) even at very low temperatures (about 100 °C) [41]. Also, the ammonium nitrate can decompose into NH_3 and HNO_3 (or NO_2 as the final product) without NO in the feed gas (Equation (4)). The results in Fig. 13 are consistent to the results reported in references [40,41]. The reaction processes, involving ads-nitrates/nitrites and lattice oxygen, follows the Equation (5)–(8). High mobility of surface lattice oxygen facilitates the formation of surface ammonium nitrates and thereby promotes the low-temperature activity of catalyst via arousing fast SCR reactions.

$$NH_4^+ + NO_3^- \leftrightarrow NO_2 + NH_3 + \text{-OH} \quad (1)$$

$$NH_4^+ + NO_3^- \leftrightarrow NH_4NO_3 \quad (2)$$

$$NO + NH_4NO_3 \rightarrow N_2 + NO_2 + 2H_2O \quad (3)$$

$$NH_4NO_3 \leftrightarrow NH_3 + NO_2 + \text{–OH} \quad (4)$$

$$2NO_2 + O^{2-} \leftrightarrow NO_2^- + NO_3^- \quad (5)$$

$$NO_3^- + NO \leftrightarrow NO_2 + NO_2^- \quad (6)$$

$$2NH_3 + NO + NO_2 \rightarrow 2N_2 + 3H_2O \quad (7)$$

$$NH_4^+ + NO_2^- \rightarrow N_2 + 2H_2O \quad (8)$$

$$NH_4NO_3 \rightarrow N_2O + 2H_2O \quad (9)$$

$$2NH_3 + 2NO + NH_4NO_3 \rightarrow 3N_2 + 5H_2O \quad (10)$$

A reason why fast SCR possesses the highest activity among SCR reactions is that the rate-determining step of fast SCR proceeds at the fastest rate (i.e., having the lowest activation barrier).

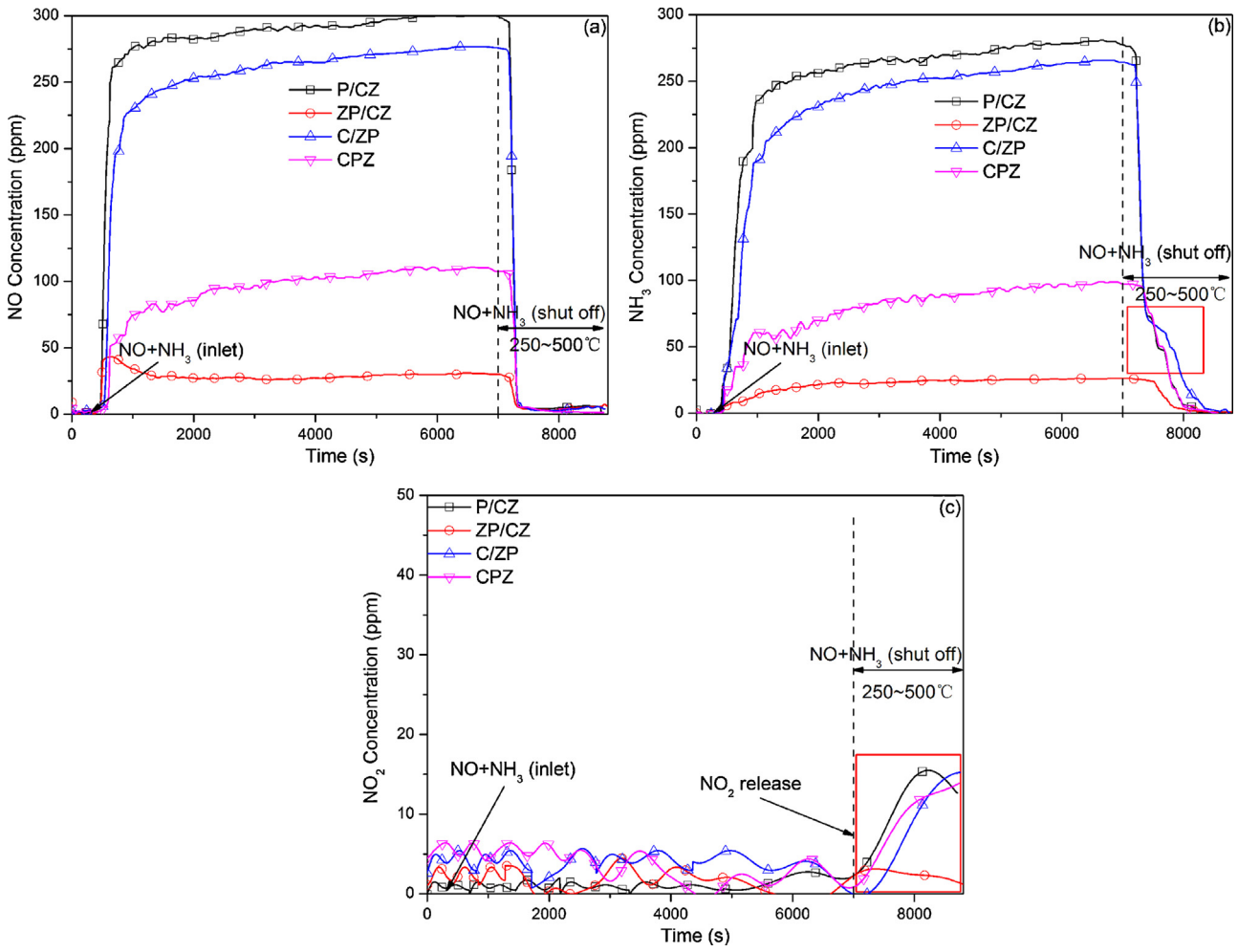

Fig. 13. NO (a), NH_3 (b) and NO_2 (c) concentration profiles of samples during the experiments: blank process (0 ~ 300 s at 250 °C, 5% O_2 in N_2); selective catalysis reaction process (300 ~ 7200 s at 250 °C, 500 ppm NH_3, 500 ppm NO, 5% O_2, 5% H_2O in N_2); temperature elevating process (7200 ~ 8800 s, from 250 °C to 500 °C, 5% O_2 in N_2).

Thus, the nitrate reduction by NO is much faster than the nitrate decomposition to N_2O (Equation (9)) and the nitrate reduction by NH_3 and NO (Equation (10)) [41]. In this work, a drastic enhancement of NO_x conversion was observed at 250 °C which is close to the temperature for thermal decomposition of ammonium nitrate (260 °C). Thus, the involvement of ammonium nitrate in the NH_3-SCR reaction (Equations (3), (7) and (10)) is responsible for the abrupt enhancement in the NO_x conversion on catalysts. The formation/decomposition of nitrites/nitrates from NO always involves the electron and/or oxygen transfer processes (Equations (11)–(14)) [42]. From UV–vis, XPS and H_2-TPR results, PZ/CZ catalyst preserves plenty of oxygen vacancies on catalyst, facilitating the electron and/or oxygen transfer on catalyst and therefore promoting the nitrites/nitrates formation and decomposition on catalyst (shown in Scheme 1.).

$$Ce^{3+}\text{–}\square + NO \rightarrow Ce^{4+}\text{–}NO^{-} \quad (11)$$

$$Ce^{4+}\text{–}NO^{-} + Ce^{4+}\text{–}O* \rightarrow Ce^{4+}\text{–}NO_2^{-} + Ce^{3+}\text{–}\square \quad (12)$$

$$Ce^{3+}\text{–}\square + NO_2 \rightarrow Ce^{4+}\text{–}NO_2^{-} \quad (13)$$

$$Ce^{4+}\text{–}NO_2^{-} + Ce^{4+}\text{–}O* \rightarrow Ce^{4+}\text{–}NO_3^{-} + Ce^{3+}\text{–}\square \quad (14)$$

where Ce^{4+}–O* is an active oxygen on ceria and Ce^{3+}–□ is an oxygen vacancy.

ZP/CZ shows almost no NH_3 and NO_2 desorption in Fig. 13. Because of the special structure of zirconium phosphate@$Ce_{0.75}Zr_{0.25}O_2$, the surface acidic zirconium phosphate can provide acid sites for NH_3 adsorption and cerium sites provide the sites for nitrate/nitrite adsorption. Two distinct adsorption sites for NH_3 and NO_x result in a close contact between ads-NH_3/NH_4^+ and ads-NO_3^-/NO_2^- species on the catalyst which can react with NO rapidly with the participation of active surface lattice oxygen and oxygen vacancy; therefore, only a small amount of ammonium nitrates deposits on the catalyst.

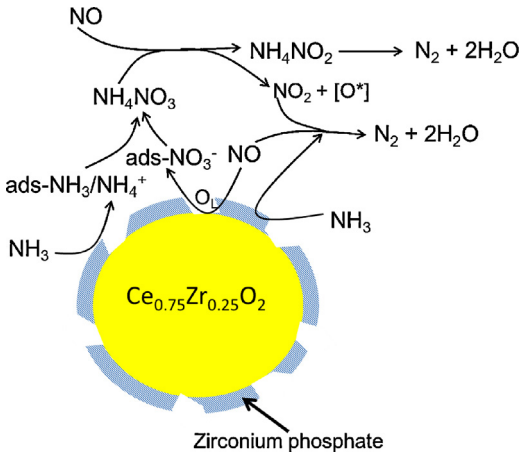

Scheme 1. NH_3-SCR reaction route on ZP/CZ.

4.3. A structural advantage of ZP/CZ sample for NH_3-SCR deNO_x

Based on the discussion above, high mobility of surface lattice oxygen and acidic surface is essential to a catalyst with high NH_3-SCR activity at low temperatures, which are the main advantage of ZP/CZ catalyst. The surface zirconium phosphate provides the adsorption sites for ammonia, while Ce^{n+} act as the redox site for NO oxidation to nitrate. Similar views were also reported in H_2-SCR of NO, where N_2 was formed by the recombination of two different in structure adjacent ads-NO_x species [43,44]. C/PZ catalyst exhibits much lower NO_x conversions in the whole temperature region due to the low acidic surface although the mobility of surface lattice oxygen is conserved. CPZ catalyst, with homogeneous distribution of Ce, Zr and PO_4^{3-} presents remarkable NO_x conversions in temperature region of 250–400 °C. The well mixing of the CeO_2, ZrO_2 and phosphate may generate less PO_4^{3-}/Ce^{n+} ratio on surface of CPZ catalyst than PZ/CZ, leading to the catalyst owns the merits of PZ/CZ and defects of C/PZ. P/CZ shows rather low NO_x conversions at low temperatures but presents remarkable high NH_3-SCR activity at much higher temperatures due to the acidic surface and inhibited mobility of surface lattice oxygen.

The NH_3-SCR reaction route can be described based on the specific structure of PZ/CZ catalyst, which is shown in Scheme 1. Gaseous NO adsorbed on cerium sites is oxidized by surface lattice oxygen to generate ads-NO_3^-. Then ads-NO_3^- species react with ads-NH_3/NH_4^+ on phosphates to yield ads-NH_4NO_3 which is further reduced by NO to generate NH_4NO_2 with the release of NO_2 and active oxygen (O*). NH_4NO_2 decompose to N_2 and H_2O. NO_2 can react with NO and NH_3 via the "fast SCR" route to generate N_2 and H_2O. Active oxygen can re-oxidize the consumed surface lattice oxygen. The O_2 can also adsorb on Ce^{3+}–□, and then be dissociated and react with oxygen vacancy to recover the O_L consumed in the NH_3-SCR reactions [45].

5. Conclusions

A novel catalyst, zirconium phosphate loading on $Ce_{0.75}Zr_{0.25}O_2$, was synthesized and exhibits high NH_3-SCR activities in a wide temperature range of 250–450 °C. Loading zirconium phosphate on $Ce_{0.75}Zr_{0.25}O_2$ can reduce the strong interaction between phosphate and cerium in addition to introducing acid sites on surface of $Ce_{0.75}Zr_{0.25}O_2$. Therefore, the mobility of surface lattice oxygen on $Ce_{0.75}Zr_{0.25}O_2$ catalyst is retained, which is essential to a catalyst with high NH_3-SCR activity at low temperatures. NH_4NO_3 is proved to be an important intermediate for NH_3-SCR reaction on ceria based catalyst. The zirconium phosphate @ $Ce_{0.75}Zr_{0.25}O_2$ catalyst preserves plenty of oxygen vacancies on the catalyst, facilitating the electron and/or oxygen transfer and therefore promoting the nitrites/nitrates formation and desorption on the catalyst. Furthermore, two distinct adsorption sites for NH_3 and NO_x result in a close contact between ads-NH_3/NH_4^+ and ads-NO_3^-/NO_2^- species on catalyst which can react with NO rapidly with the participation of active surface lattice oxygen and oxygen vacancy; therefore, only a small amount of ammonium nitrates deposits on the catalyst, which facilitates the low-temperature NH_3-SCR activity of the catalyst.

Acknowledgments

The authors would like to acknowledge the National Natural Science Foundation of China for financial support of Project 51202126. Moreover, we would also thank the financial support from Postdoctoral Science Foundation of China (2012M520266) and Strategic Emerging Industry Development Funds of Shenzhen (JCYJ20120619152738634).

Appendix A. Supplementary data

Supplementary data associated with this article can be found, in the online version, at http://dx.doi.org/10.1016/j.apcatb.2014.08.006.

References

[1] H. Bosh, F. Janssen, Catal. Today 2 (1988) 369–379.
[2] K.C. Taylor, Catal. Rev. Sci. Eng. 35 (1993) 457–481.
[3] K. Skalska, J.S. Miller, S. Ledakowicz, Sci. Total Environ. 408 (2010) 3976–3989.
[4] C. Ciardelli, I. Nova, E. Tronconi, D. Chatterjee, B. Bandl-Konrad, M. Weibel, B. Krutzsch, Appl. Catal. B: Environ. 70 (2007) 80–90.
[5] G. Busca, L. Lietti, G. Ramis, F. Berti, Appl. Catal. B: Environ. 18 (1998) 1–36.
[6] N.Y. Topsoe, H. Topsoe, J.A. Dumesic, J. Catal. 151 (1995) 226–240.
[7] A. Grossale, I. Nova, E. Tronconi, Catal. Today 136 (2008) 18–27.
[8] W.P. Shan, F.D. Liu, H. He, X.Y. Shi, C.B. Zhang, Catal. Today 184 (2012) 160–165.
[9] L. Chen, J.H. Li, M.F. Ge, Environ. Sci. Technol. 44 (2010) 9590–9596.
[10] Z.M. Liu, S.X. Zhang, J.H. Li, L.L. Ma, Appl. Catal. B: Environ. 144 (2014) 90–95.
[11] Z.C. Si, D. Weng, X.D. Wu, Z.R. Ma, J. Ma, R. Ran, Catal. Today 201 (2013) 122–130.
[12] Z.C. Si, D. Weng, X.D. Wu, R. Ran, Z.R. Ma, Catal. Commun. 17 (2012) 146–149.
[13] Y. Peng, K.Z. Li, J.H. Li, Appl. Catal. B: Environ. 140 (2013) 483–492.
[14] L. Zhang, J. Pierce, V.L. Leung, D. Wang, W.S. Epling, J. Phys. Chem. C 117 (2013) 8282–8289.
[15] Y. Peng, R.Y. Qu, X.Y. Zhang, J.H. Li, Chem. Commun. 49 (2013) 6215–6217.
[16] R.Y. Qu, X. Gao, K.F. Cen, J.H. Li, Appl. Catal. B: Environ. 142 (2013) 290–297.
[17] T.T. Gu, Y. Liu, X.L. Weng, H.Q. Wang, Z.B. Wu, Catal. Commun. 12 (2010) 310–313.
[18] G. Bagnasco, G. Busca, P. Galli, M.A. Massucci, K. Melanová, P. Patrono, G. Ramis, M. Turco, Appl. Catal. B: Environ. 28 (2000) 135–142.
[19] R. Hernández-Huesca, J. Santamarıa-González, P. Braos-Garcıa, P. Maireles-Torres, E. Rodrıguez-Castellón, A. Jiménez-López, Appl. Catal. B: Environ. 29 (2001) 1–11.
[20] R. Hernández-Huesca, P. Braos-Garcıá, J. Mérida-Robles, P. Maireles-Torres, E. Rodrıguez-Castellón, A. Jiménez-López, Chemosphere 48 (2002) 467–474.
[21] Z.C. Si, D. Weng, X.D. Wu, J. Yang, B. Wang, Catal. Commun. 11 (2010) 1045–1048.
[22] L.J. Alemany, L. Lietti, N. Ferlazzo, P. Forzatti, G. Busca, E. Giamello, F. Bregani, J. Catal. 155 (1995) 117–130.
[23] Z. Wang, Z.P. Qu, X. Quan, Z. Li, H. Wang, R. Fan, Appl. Catal. B: Environ. 134 (2013) 153–166.
[24] C. Larese, F.C. Galisteo, M.L. Granados, R. Mariscal, J. Fierro, M. Furió, R.F. Ruiz, Appl. Catal. B: Environ. 40 (2003) 305–317.
[25] L. Xu, G. Guo, D. Uy, A.E. O'neill, W.H. Weber, M.J. Rokosz, R.W. McCabe, Appl. Catal. B: Environ. 50 (2004) 113–125.
[26] C. Larese, M. López Granados, R. Mariscal, J. Fierro, P.S. Lambrou, A.M. Efstathiou, Appl. Catal. B: Environ. 59 (2005) 13–25.
[27] Q. Zhang, Q. Du, T. Jiao, B. Pan, Z. Zhang, Q. Sun, S. Wang, T. Wang, F. Gao, Chem. Eng. J. 221 (2013) 315–321.
[28] H. Hirai, T. Masui, N. Imanaka, G. Adachi, J. Alloys Compd. 374 (2004) 84–88.
[29] K. Rajesh, P. Mukundan, P.K. Pillai, V.R. Nair, K.G.K. Warrier, Chem. Mater. 16 (2004) 2700–2705.
[30] A. Tarafdar, A.B. Panda, N.C. Pradhan, P. Pramanik, Microporous Mesoporous Mater. 95 (2006) 360–365.
[31] R. Si, Y.W. Zhang, L.P. You, C.H. Yan, Angew. Chem. 117 (2005) 3320–3324.
[32] B. Choudhury, A. Choudhury, Mater. Chem. Phys. 131 (2012) 666–671.
[33] B. Tatar, E.D. Sam, K. Kutlu, M. Ürgen, J. Mater. Sci. 43 (2008) 5102–5108.
[34] A.A. Battiston, J.H. Bitter, D.C. Koningsberger, J. Catal. 218 (2003) 163–177.
[35] W.P. Shan, F.D. Liu, H. He, X.Y. Shi, C.B. Zhang, Appl. Catal. B: Environ. 115–116 (2012) 100–106.
[36] Y. Wang, F. Wang, Y. Chen, D.F. Zhang, B. Li, S.F. Kang, X. Li, L.F. Cui, Appl. Catal. B: Environ. 147 (2014) 602–609.
[37] J. Zhu, J. Yang, Z.F. Bian, J. Ren, Y.M. Liu, Y. Cao, H.X. Li, H.Y. He, K.N. Fan, Appl. Catal. B: Environ. 76 (2007) 82–91.
[38] S.Y. Christou, M.C. Alvarez-Galvan, J.L.G. Fierro, A.M. Efstathiou, Appl. Catal. B: Environ. 106 (2011) 103–113.
[39] L. Lietti, Appl. Catal. B: Environ. 10 (1996) 281–297.
[40] I. Nova, C. Ciardelli, E. Tronconi, D. Chatterjee, B. Bandl-Konrad, Catal. Today 114 (2006) 3–12.
[41] A. Savara, M.J. Li, W.M. Sachtler, E. Weitz, Appl. Catal. B: Environ. 81 (2008) 251–257.
[42] I. Atribak, B. Azambre, A. Bueno López, A. García-García, Appl. Catal. B: Environ. 92 (2009) 126–137.
[43] C.N. Costa, A.M. Efstathiou, J. Phys. Chem. C 111 (2007) 3010–3020.
[44] C.N. Costa, A.M. Efstathiou, J. Phys. Chem. B 108 (2004) 2620–2630.
[45] C. Binet, M. Daturi, J.C. Lavalley, Catal. Today 50 (1999) 207–225.